

Temperature dependence of linewidth in nano-contact based spin torque oscillators: effect of multiple oscillatory modes

P. K. Muduli*

*Department of Physics, University of Gothenburg, 41296 Gothenburg, Sweden and
Department of Physics, Indian Institute of Technology Delhi, New Delhi, 110016, India*

O. G. Heinonen

*Materials Science Division, Argonne National Laboratory, Lemont, IL 60439, USA and
Department of Physics and Astronomy, Northwestern University, 2145 Sheridan Rd., Evanston, IL 60208-3112*

Johan Åkerman

*Physics Department, University of Gothenburg, 41296 Gothenburg, Sweden and
Materials Physics, School of ICT, KTH-Royal Institute of Technology, Electrum 229, 164 40 Kista, Sweden*

We discuss the effect of mode transitions on the current (I) and temperature (T) dependent linewidth (Δf) in nanocontact based spin torque oscillators (STOs). At constant I , Δf exhibits an anomalous temperature dependence near the mode transitions; Δf may either increase or decrease with T depending on the position w.r.t. the mode transition. We show that the behavior of Δf as a function of I can be fitted by the single mode analytical theory of STOs, even though there are two modes present near the mode transition, if the nonlinear amplification is determined directly from the experiment. Using a recently developed theory of two *coupled* modes, we show that the linewidth near mode transition can be described by an “effective” single-oscillator theory with an enhanced nonlinear amplification that carries additional temperature dependence, which thus qualitatively explain the experimental results.

PACS numbers: 85.75.-d, 76.50.+g, 72.25.-b

I. INTRODUCTION

A spin-polarized current traversing a thin magnetic layer can exert a significant torque on the magnetization through the spin transfer torque (STT) effect.¹⁻⁷ The effect can be described as negative damping, linearly proportional to the spin-polarized current, which at a certain threshold can overcome the natural Gilbert damping in the magnetic layer, allowing for coherent, large amplitude, excitation of spin waves. If the magnetic layer is part of a structure with magnetoresistance, such as a spin valve (SV) or a magnetic tunnel junction (MTJ), the excited spin waves can be used to generate a current- and field-tunable microwave voltage signal; the resulting device is commonly called a spin torque oscillator (STO).⁸ Interest in STOs for microwave applications is steadily increasing, due to their attractive combination of very large frequency tuning ranges,⁹⁻¹¹ efficient spin-wave emission in magnonic devices,¹²⁻¹⁴ very high modulation rates,¹⁵⁻²³ sub-micron footprints,²⁴ and straightforward integration with semiconductor technology using the same processes as magnetoresistive random access memory.^{25,26}

A minimal spectral linewidth, Δf , of the microwave signal is highly desirable for applications. While a number of recent experimental studies have addressed the temperature dependence of Δf in nanopillar STOs²⁷⁻³² the study of the temperature dependent linewidth in nanocontact STOs is limited to a recent work by Schneider *et. al.*³³ The theory of the origin of STO linewidths and their temperature dependence is now well established

for single spin-wave modes.³⁴⁻³⁹ A key result is the strong impact that limited amplitude noise can have on the STO phase noise, via the strong amplitude-phase coupling. Gaussian (white) amplitude noise is transformed into colored phase noise, and the intrinsic Lorentzian line shape expected for an auto-oscillator with zero amplitude-phase coupling changes into a convolution of Lorentzian and Gaussian line shapes.⁴⁰ The coupling also leads to a substantial enhancement, or amplification, of the thermal broadening, and can also lead to asymmetric line shapes near threshold.³⁶ The degree of coloring should also change with temperature, leading to a crossover from a linear temperature dependence of Δf at low temperature, to a square root dependence at high temperature.³⁷

All temperature dependent studies to date show temperature regions with unexpected behavior. In Ref. 29, Δf in the subthreshold regime narrows by a factor of 6, from 1.2 GHz to 200 MHz, when the temperature is raised from 20 K to 140 K. In Ref. 28, the slope of the temperature dependence even changes sign multiple times as a function of drive current, and is close to zero at the smallest Δf . In Ref. 27, Δf increases exponentially above a certain temperature; the concept of mode hopping was introduced to explain and model this dependence. The origin of these rather complex temperature dependencies is yet to be explained. More recently, a linear behavior of linewidth is observed for a certain range of temperature in magnetic tunnel junction based STOs.^{31,32} A saturation of linewidth is observed in both these studies for temperature below 100 K, which is not explained by the existing theories. In addition, the temperature de-

pendence of power restoration rate observed in Ref 32 can not be explained by the single mode theory.³⁸ Thus the details of the temperature dependence of linewidth in STOs is far from being understood.

In this work, we present a detailed study of the temperature-dependent linewidth in nanocontact STOs. While all measurements were carried out at current and magnetic field values where only propagating spin waves were generated,^{12,41} we found a large number of mode transitions as a function of current (at a fixed temperature T) and temperature (at a fixed current I). The measured linewidth is highly nonmonotonic both as a function of current and of temperature, with large enhancements at currents or temperatures where mode transitions occurred. We show that the linewidth is very well fitted by the single oscillator theory^{37,38}, if the so-called amplification factor is obtained directly from measurements. While this agreement is similar to that of Refs. 19 and 29, we find the temperature dependence of the linewidth does not agree with that obtained directly from calculations using the nonlinear single-oscillator theory^{37,38}, from which typically a linear dependence on T is obtained for the systems under study here. These observations indicate that the central mechanism for linewidth broadening in nonlinear single-oscillator theory applies here, too: The linewidth is driven by phase noise amplified by the coupling through the nonlinear frequency shift to power amplitude fluctuations. However, our results indicate that this coupling may itself have a nontrivial temperature (and current) dependence, especially near mode transitions. We will here show that extending the nonlinear single-oscillator theory to include two coupled modes⁴² leads to additional couplings between the phase and power fluctuations. Under some simplifying assumptions, these couplings lead to a changed power restoration rate and the final result for the linewidth looks very much like that from the nonlinear single-oscillator theory^{37,38}, but with an enhanced nonlinear amplification that carries additional temperature dependence. This explains qualitatively the observed temperature dependence of the linewidth near mode transitions.

II. EXPERIMENT

The results presented in this work are from a single nanocontact STO device with an e-beam patterned $50 \times 150 \text{ nm}^2$ elliptical nanocontact fabricated on top of a $8 \times 26 \text{ }\mu\text{m}^2$ pseudo-spin-valve mesa based on $\text{Co}_{81}\text{Fe}_{19}$ (20 nm)/Cu(6 nm)/ $\text{Ni}_{80}\text{Fe}_{20}$ (4.5 nm), as described in Ref. 43. While not shown here, other nanocontacts of varying sizes were also studied as a function of temperature, and gave the same qualitative results.

The experimental circuit is similar to that employed in Refs. 10 and 44. The signal generated from the STO was amplified using a broadband +22-dB microwave amplifier, and detected by a 20 Hz-46 GHz Rohde & Schwarz

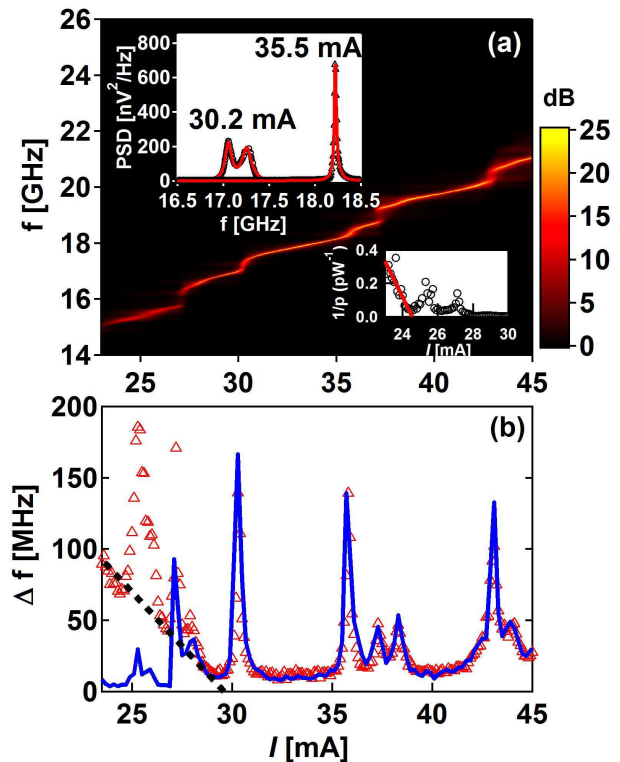


Figure 1. (Color online)(a) Two-dimensional power spectral density map of f versus I at a magnetic field of $\mu_0 H = 1 \text{ T}$, applied at an angle of 80° to the film plane. Top inset shows two examples of mode transitions at $I = 30.2 \text{ mA}$ and 35.3 mA respectively, where the left spectrum has two clearly resolved Lorentzian peaks, and the right spectrum shows a single broader, asymmetric peak that can still be well fitted by two Lorentzian functions. The bottom inset shows the inverse power $1/p$ vs current and a linear fit (solid line). (b) Experimentally measured (red triangles) and calculated Δf (blue solid line). The black dashed line represents a linear fit to linewidth using Eq.(1) for subthreshold currents.

FSU46 spectrum analyzer. The measurement was performed in the default mode of the spectrum analyzer, mode for spectrum analysis, the so-called analyzer mode. We use a resolution bandwidth of 10 MHz and video bandwidth of 10 kHz. The spectra were measured in the frequency range 13-25 GHz with a sweep time of 100 ms. We also average 20 traces resulting in a total measurement time of about 6.4 s. The dc bias current is fed to the device by a current source through a 0-26 GHz bias tee connected in parallel with the transmission line. The temperature of the sample was varied in the range 300-400 K through use of a heating foil underneath the sample. Each measurement temperature was maintained with a precision of 0.1 K using a thermocouple attached to the bottom of the sample and a software-based PID controller. All measurements were performed in a $\mu_0 H = 1 \text{ T}$ field applied at an angle of 80° w.r.t. the film plane. In this geometry only a propagating spin wave mode^{12,14,45,46} is excited, and the output power is close

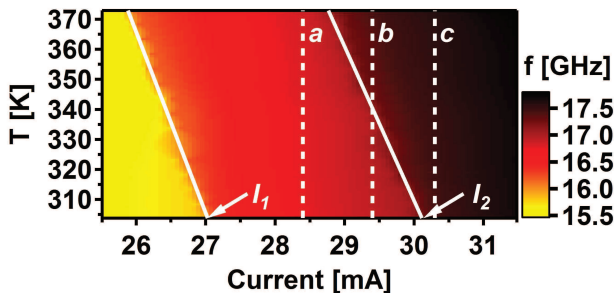


Figure 2. (Color online) Map of frequency of the strongest mode versus temperature and bias I , showing the mode transition with temperature. The solid lines are linear fits to the threshold current for the mode transitions I_1 and I_2 versus temperature. The dotted lines are the positions at which the behavior of the linewidth is discussed in Fig. 3.

to its maximum value.¹⁰

III. RESULTS

Figure 1 shows the current (I) dependence of the STO frequency at room temperature. In addition to the expected linear blue shift with I , a large number of discontinuous jumps and other nonlinearities can be observed. We argue that all these nonlinear features are related to mode transitions, some large, where two distinct peaks can be observed on the spectrum analyzer [the left spectrum in the inset of Fig. 1(a)], and others small, where only a single peak is observed, though with a significant increase in both nonlinearity and linewidth [the right spectrum in the inset of Fig. 1(a)]. Similar mode transitions have been observed in the literature^{27,47,48} and numerical simulations have reproduced this behavior for in-plane fields.⁴⁹

The mode transitions have a significant impact on Δf vs. I , as shown in Fig. 1 (b). We define Δf as the full width at half maximum (FWHM) obtained by fitting a single Lorentzian function. In the case of two modes, we use the linewidth of the strongest mode (the mode with the highest output power). In the subthreshold regime, Δf decreases linearly with increasing I , which we attribute to the narrowing of the natural ferromagnetic resonance (FMR) linewidth under the influence of the negative damping associated with spin torque.^{35,38} At every mode transition position, we also observe a dramatic increase in Δf leading to a highly nonlinear dependence on I . It is noteworthy that a strong mode transition, and the associated increase in Δf , can also be observed well inside the subthreshold regime, at about 25 mA. The existence of mode transitions is hence not limited to states of steady precession, as in Ref. 49.

In order to show the effect of temperature on mode transitions, we plot a map of measured frequency vs temperature and current, as shown in Fig. 2. At room temperature these transitions are located at about $I_1=27$ mA

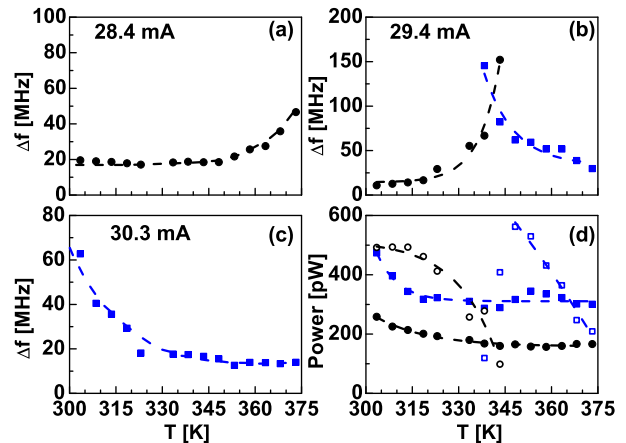


Figure 3. (Color online) Measured linewidth versus temperature at (a) 28.4 mA, (b) 29.4 mA, and (c) 30.3 mA. The solid black circles (respectively the solid blue squares) denote the mode excited below (above) $I_2=30$ mA at room temperature. (d) Integrated power versus temperature at 28.4 mA (solid black circles), 29.4 mA (open symbols), and 30.3 mA (solid blue squares). The dashed lines serve as visual aids.

and $I_2=30$ mA. As T is increased, both I_1 and I_2 move to lower values following a linear dependence (the solid lines in Fig. 2). This T dependence of I_1 and I_2 has direct consequences for $\Delta f(T)$. To illustrate this, we have chosen three current values, shown by the dashed lines in Fig. 2, which lie below, on top of, and above the second mode transition. Figures 3 (a)– 3(c) show Δf vs. T at these three currents, which clearly exhibit three dramatically different T dependencies: i) at 28.4 mA, we observe a nonlinear increase of Δf with T , ii) at 29.4 mA, we observe a nonmonotonic T dependence, and iii) at 30.3 mA we observe a nonlinear *decrease* in Δf with T . It is quite obvious that none of the measured curves in Fig. 3 follow either a linear or a square-root T dependence, as expected from the theories of thermally induced phase noise.^{27,35,38,39}

Now we will compare our results with the single mode analytical theory.^{35,38} According to this theory, Δf of a nonlinear oscillator is given by

$$\Delta f = \Gamma_g \left(1 - \frac{I}{I_{\text{th}}}\right), \text{ for } I \ll I_{\text{th}} \quad (1)$$

$$= \Delta f_L (1 + \nu^2), \text{ for } I \gg I_{\text{th}}, \quad (2)$$

where Γ_g is the natural FMR linewidth, I the bias current, I_{th} the threshold current, and the nonlinear linewidth amplification is $(1 + \nu^2) = 1 + \left(\frac{p_0 N}{\Gamma_p}\right)^2$, where $N = \frac{d\omega}{dp}$ is the nonlinear frequency shift, and Γ_p is the power restoration rate (Γ_p^{-1} is the correlation time of the power fluctuations); $\Delta f_L = \Gamma_g \frac{kT}{E(p_0)}$ is the intrinsic thermal linewidth, i.e., the linewidth of a linear ($\nu = 0$) oscillator. Here, $E(p_0)$ is the total energy of the oscillator. Above threshold ($I \gg I_{\text{th}}$), the nonlinear amplification of the linewidth is controlled by the ratio of the nonlinear frequency shift N to the power restoration rate

Γ_p . The reason for this^{35,38} is that power fluctuations couple to phase fluctuations through the nonlinear frequency shift N , and the linewidth is dominated by phase fluctuations. The linewidth increases when N is large, so that small power fluctuations give rise to large phase fluctuations, or if Γ_p is small, so that power fluctuations remain for a long time during which they affect phase fluctuations. For the nanocontact under study, the nonlinear damping Q is small³⁰, and we can approximate $(1 + \nu^2) \approx 1 + \left(\frac{I}{\Gamma_g} \frac{df}{dI}\right)^2$.

We first compare our experimental results for fixed T with theory.^{35,38} In order to do so, we need to extract Γ_g . We fit the initial decrease in linewidth with Eq. (1), and obtain $\Gamma_g = (500 \pm 20)$ MHz and $I_{th} = (29 \pm 1)$ mA, as shown by the dashed line in Fig. 1 (b). Next, from the measured f vs I , we obtain df/dI and directly calculate the nonlinear amplification factor $(1 + \nu^2)$, and find from a fit to Eq. (2) that $\Delta f_L \sim 67$ kHz, for $I > I_{th}$. This value of Δf_L corresponds to $kT/E(p_0) \sim 1.5 \times 10^{-4}$. As shown in Fig. 1 (b), the calculated Δf shows very good agreement with the experimentally measured linewidth, and also reproduces the dramatic increase in Δf which occurs around each mode transition. The agreement indicates that the nonlinear amplification of the linewidth is controlled by the nonlinear frequency shift $N \propto df/dI$, while the power restoration rate Γ_p is constant. The agreement is lost for $I < 27$ mA, as expected for currents below threshold.^{35,38} We have also used the inverse power method⁵⁰ to determine the threshold current as shown in the inset of Fig. 1 (a). A fit of this data for current below 25 mA is shown by the solid line. From this fit it appears as if the STO is close to auto-oscillation already at about 24.5 mA, but gets interrupted by one or more subthreshold mode transitions. It is only at about 27-28 mA that robust auto-oscillation begins.

Next, we want to compare the temperature dependence (at fixed I) of Δf_L and $(1 + \nu^2)$ as obtained from the experiment with theoretical predictions^{35,38}. According to the theory, $\Delta f_L(T)$ should be proportional to T , since it is the linewidth of a linear oscillator in contact with a thermal bath, while $(1 + \nu^2)$ has a monotonic temperature dependence. Using the agreement between the calculated and measured linewidths in Fig. 1, we can now extract Δf_L and its temperature dependence, as shown in Fig. 4(a). Since the determination of $(1 + \nu^2)$ is more accurate in regions between mode transitions, i.e., where df/dI do not diverge, we use the average value of Δf_L for $30.5 \text{ mA} < I < 31.5 \text{ mA}$, which excludes any mode transitions and is above threshold at all temperatures. A linear increase in Δf_L with T is observed. The solid and dashed lines are calculations based on the classical quasi-Hamiltonian formalism for spin waves,^{35,36,38,51,52} which shows reasonable agreement with the experiment and also predicts a linear behavior similar to experiment even with the inclusion of the temperature dependence of M_0 in the calculation (red solid line). This calculation assumes single mode excitation but considers the nonuni-

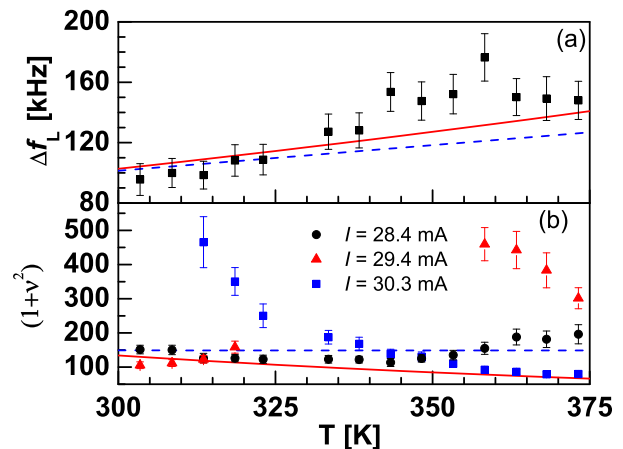


Figure 4. Temperature dependence of (a) extracted linear contribution of linewidth Δf_L (solid symbols) and (b) the nonlinear amplification, $(1 + \nu^2)$ (solid and open symbols). The solid red lines are calculation based with inclusion of temperature dependence of M_s , where as the dashed blue lines are calculation assuming no temperature dependence of M_s .

form nature of propagating spin waves by "exchange normalization" of magnetic field, and normalization of volume under the nanocontact.³⁸ The parameters used are similar to those of Ref. 12, the electron gyromagnetic factor: $\gamma = 1.76 \times 10^7$ rad/Oe, saturation magnetization: $M_0(300K) = 640$ emu/cm³, Gilbert damping parameter: $\alpha_G = 0.01$, dimensionless spin-polarization efficiency: $\epsilon = 0.2$, the exchange length: $\lambda_{ex} = 5$ nm, and $(I/I_{th})_{300K} = 5$. The effective volume V_{eff} is assumed to be 1.5 times that of the volume under the nanocontact. We use $\Gamma_g = (500 \pm 20)$ MHz, as determined from the experiment. Calculation also predicts $\Gamma_g = 500$ MHz for our experimental geometry. We note that the agreement with Δf_L with T was obtained only when $I/I_{th} > 5$. We attribute this to the fact that the analytical Eq. (2) is an asymptotic equation that is valid only for $I \gg I_{th}$.³⁵ Basically we treated I/I_{th} as a fitting parameter, with the other parameters kept fixed at their reasonable values, since the precise values of these parameters are a bit uncertain.

In Fig. 4(b) we show the behavior of measured $(1 + \nu^2)$ vs T (symbols) for the three current values of 28.4 mA, 29.4 mA and 30.3 mA along with the calculated behavior for $I/I_{th} = 5$ (solid and dashed lines). The experimental behavior of $(1 + \nu^2)$ vs T is dramatically different for the three cases but very similar to the behavior of the linewidth as a function of T shown in Fig 3. In contrast, the calculations of single-mode theory predict a monotonic decrease of $(1 + \nu^2)$ with T when the temperature dependence of M_s is included. Hence the calculations agree with the experiment only for a limited range of temperature and when the STO is far from the mode transition. For example, at 28.4 mA (30.3 mA), $(1 + \nu^2)$ is enhanced at higher (lower) temperature, which is close to the mode transition. Detail examination show that

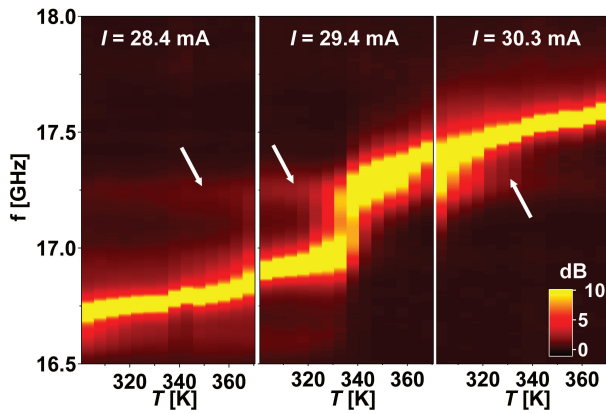


Figure 5. Map of power (dB) vs frequency (f) and temperature T for the three example current values of 28.4 mA, 29.4 mA, and 30.3 mA. The arrows indicate the presence of additional modes, the amplitude of which depends on temperature.

this enhancement occurs when two modes are observed.

$$\begin{aligned} \frac{dc_1}{dt} + i\omega_1(p_1, p_2)c_1 + [\Gamma_+(p_1, p_2) - \Gamma_-(p_1, p_2)]c_1 - ke^{i\varphi}c_2 &= 0 \\ \frac{dc_2}{dt} + i\omega_2(p_1, p_2)c_2 + [\Gamma_+(p_1, p_2) - \Gamma_-(p_1, p_2)]c_2 - ke^{i\varphi}c_1 &= 0. \end{aligned} \quad (3)$$

Here, Γ_+ and Γ_- are the positive and negative damping, and ω_1 and ω_2 the mode-frequencies; we have indicated the dependence of ω_i , Γ_+ , and Γ_- on the mode powers p_1 and p_2 . The equations contain a linear coupling term with complex amplitude $ke^{i\varphi}$, with k real and $k \geq 0$. This term is not allowed on short time scales if $\omega_1 \neq \omega_2$. Here, however, we are interested in behavior over times much larger than the time-scale of the periods of the modes or of thermal fluctuations. In that case, the coupling mediated through the linear coupling describes processes in which one mode can decay into the other through intermediate states and energy that is absorbed or released into other magnetic modes or a thermal reservoir. Such a process becomes more likely as the mode frequencies approach each other, with a concomitant increase in k . The experiments show a significant current and temperature dependence of the main mode frequency. Therefore, the linear mode coupling also has a strong current and temperature dependence, $k = k(I, T)$ and $\varphi = \varphi(I, T)$. In particular, the magnitude of k has maxima at currents and temperatures at which mode transitions occur. We will see that this coupling plays a key role.

We now make some simplifying assumptions. First, we assume that the mode frequency ω_i only depends on p_i and not on p_j , $j \neq i$. Next, we assume that the system is

This can be clearly seen in Fig. 5 which shows the measured power vs frequency (f) and temperature T for the three current values. These spectra show the presence of an additional mode (as shown by the arrows) for all these currents. The temperature dependence of the amplitude of this additional mode has a clear correlation with the behavior of $(1 + \nu^2)$ vs T in Fig. 4(b). For example, the amplitude of second mode increases (decreases) with temperature at 28.4 mA (30.3 mA). Thus our results indicate that when two modes are observed, the experimental $(1 + \nu^2)$ is enhanced compared to the prediction of single mode calculation.

IV. DISCUSSION

We will now discuss the mechanism for the anomalous temperature dependence of the linewidth. The basic assumption is that in the presence of two mode, mode coupling near a transition can lead to an increase in the linewidth. The starting point is a set of coupled equations for the complex amplitudes c_i , $i = 1, 2$ of the time-dependence of the modes,⁴²

close to, but above, threshold (recall that the threshold current is about 27 mA and the relevant current values are around 30 mA). We then expand Eq. (3) near $c_i = 0$ and write the equations in terms of power amplitude and phase, $c_i = \frac{Q_i}{\sqrt{\omega_i}} e^{-i(\omega_{i,0}t - \varphi_i)}$, where $\omega_{i,0}$ is the threshold mode frequency. This leads to the following equations for the time dependence of the amplitudes Q_i and phases φ_i :

$$\begin{aligned} \frac{dQ_1}{dt} &= \Gamma_g(I/I_{\text{th}} - 1)Q_1 - (\overline{Q}Q_1^2 + \overline{P}Q_2^2)Q_1 \\ &\quad + kQ_2\sqrt{\frac{\omega_{1,0}}{\omega_{2,0}}}\cos(\varphi - \varphi_2 + \varphi_1) \end{aligned} \quad (4a)$$

$$\begin{aligned} \frac{dQ_2}{dt} &= \Gamma_g(I/I_{\text{th}} - 1)Q_2 - (\overline{Q}Q_2^2 + \overline{P}Q_1^2)Q_2 \\ &\quad + kQ_1\sqrt{\frac{\omega_{2,0}}{\omega_{1,0}}}\cos(\varphi - \varphi_2 - \varphi_1) \end{aligned} \quad (4b)$$

$$\frac{d\varphi_1}{dt} = -N_1Q_1^2 + k\frac{Q_2}{Q_1}\sqrt{\frac{\omega_{1,0}}{\omega_{2,0}}}\sin(\varphi + \varphi_2 - \varphi_1) \quad (4c)$$

$$\frac{d\varphi_2}{dt} = -N_2Q_2^2 + k\frac{Q_1}{Q_2}\sqrt{\frac{\omega_{2,0}}{\omega_{1,0}}}\sin(\varphi - \varphi_2 + \varphi_1). \quad (4d)$$

Here, N_i is the nonlinear frequency shift, I_{th} the threshold current, and \overline{Q} and \overline{P} the diagonal and off-diagonal nonlinear damping coefficients, respectively. We will for

simplicity assume that $N_1 = N_2 = N$.

Next, we introduce the transformations⁵³ $Q_1 = \sqrt{p} \cos\left(\frac{\theta+\pi/2}{2}\right)$ and $Q_2 = \sqrt{p} \sin\left(\frac{\theta+\pi/2}{2}\right)$, where p is the total power in the two modes. These transformations recast the description of the mode amplitudes Q_i in terms

$$\begin{aligned} \frac{d(p_0 + \delta p)}{dt} = & 2(I/I_{\text{th}} - 1)\Gamma_g(p_0 + \delta p) - 2\bar{Q}(p_0^2 + 2p_0\delta p) - (\bar{P} - \bar{Q})\cos^2\theta(p_0^2 + 2p_0\delta p) \\ & + k(p_0 + \delta p)\cos\theta\left[\sqrt{\frac{\omega_{1,0}}{\omega_{2,0}}}\cos(\varphi + \psi) + \sqrt{\frac{\omega_{2,0}}{\omega_{1,0}}}\cos(\varphi - \psi)\right], \end{aligned} \quad (5)$$

where $\psi = \varphi_2 - \varphi_1$, with a time evolution given by

$$\frac{d\psi}{dt} = -Np_0\sin\theta - N\delta p\sin\theta + k\frac{1 - \sin\theta}{\cos\theta}\sqrt{\frac{\omega_{2,0}}{\omega_{1,0}}}\sin(\varphi - \psi) - k\frac{1 + \sin\theta}{\cos\theta}\sqrt{\frac{\omega_{1,0}}{\omega_{2,0}}}\sin(\varphi + \psi) \quad (6)$$

Ignoring fluctuations for the moment, and keeping in mind that the power p_0 is constant, the equations (5) and (6) describe a two-dimensional dynamically driven system in (θ, ψ) -space. The system under consideration here has, far away from a mode transition so that $k \approx 0$, a single stable fixed point $\theta = -\pi/2$ ($\theta = \pi/2$) with all power in mode ω_1 (ω_2) well below (above) the mode

of p and θ , where p is total power and θ describes how the power is distributed between the two modes. Inserting these in Eqs. (4a) and (4b) and assuming that the *average* power p_0 is stationary and writing $p = p_0 + \delta p$, with $dp_0/dt = 0$ and δp the power fluctuations, we obtain the following linearized equation for the power (linearized in power fluctuations about the average power p_0):

transition. Near or at the mode transition, the system may have stable fixed points, unstable fixed points, or limit cycles. In either case we will assume that the experimental linewidth arises from fluctuations in the *total* power and phase difference, and we will therefore ignore fluctuations in θ . By enforcing the stationarity condition $dp_0/dt = 0$ we obtain from Eq. (5)

$$2(I/I_{\text{th}} - 1)\Gamma_g - 2\bar{Q}p_0 - (\bar{P} - \bar{Q})p_0\cos^2\theta + kp_0\cos\theta\left[\sqrt{\frac{\omega_{1,0}}{\omega_{2,0}}}\langle\cos(\varphi + \psi)\rangle + \sqrt{\frac{\omega_{2,0}}{\omega_{1,0}}}\langle\cos(\varphi - \psi)\rangle\right] = 0, \quad (7)$$

where $\langle \dots \rangle$ denotes a suitable time-average over times long compared to the time scale of fluctuations (*e.g.*, a limit cycle). Inserting this into Eq. (5), and separating ψ into a regular part Ψ , describing the slow time evolution of the phase difference of the two modes, and fluctua-

tions $\delta\psi$, $\psi = \Psi + \delta\psi$, and replacing $\cos\psi$ ($\sin\psi$) with $\langle\cos\Psi\rangle$ ($\langle\sin\Psi\rangle$) we obtain the following linearized equations relating the fluctuations in power and phase angle difference:

$$\begin{aligned} \frac{d\delta p}{dt} = & 2(I/I_{\text{th}} - 1)\Gamma_g\delta p - 4\bar{Q}p_0\delta p + 2(\bar{P} - \bar{Q})\cos^2\theta\delta p + k\delta p\cos\theta\left[\sqrt{\frac{\omega_{1,0}}{\omega_{2,0}}}\langle\cos(\varphi + \Psi)\rangle + \sqrt{\frac{\omega_{2,0}}{\omega_{1,0}}}\langle\cos(\varphi - \Psi)\rangle\right] \\ & - kp_0\cos\theta\delta\psi\left[\sqrt{\frac{\omega_{1,0}}{\omega_{2,0}}}\langle\sin(\varphi + \Psi)\rangle - \sqrt{\frac{\omega_{2,0}}{\omega_{1,0}}}\langle\sin(\varphi - \Psi)\rangle\right], \end{aligned} \quad (8)$$

and

$$\begin{aligned} \frac{d\delta\psi}{dt} = & -N\delta p\sin\theta \\ & -k\delta\psi\frac{1 - \sin\theta}{\cos\theta}\sqrt{\frac{\omega_{2,0}}{\omega_{1,0}}}\langle\cos(\varphi - \Psi)\rangle \\ & -k\delta\psi\frac{1 + \sin\theta}{\cos\theta}\sqrt{\frac{\omega_{1,0}}{\omega_{2,0}}}\langle\cos(\varphi + \Psi)\rangle \end{aligned} \quad (9)$$

with Ψ satisfying

$$\begin{aligned} \frac{d\Psi}{dt} = & -Np_0\sin\theta \\ & + k\frac{1 - \sin\theta}{\cos\theta}\sqrt{\frac{\omega_{2,0}}{\omega_{1,0}}}\sin(\varphi - \Psi) \\ & - k\frac{1 + \sin\theta}{\cos\theta}\sqrt{\frac{\omega_{1,0}}{\omega_{2,0}}}\sin(\varphi + \Psi). \end{aligned} \quad (10)$$

We pause for a moment to note that Eqs. (8) to (10) restricted to a single mode ($k = 0$ and $\cos\theta = 0$) are precisely the results of Kim, Slavin, and Tiberkevich^{36,38,51,52}, with $\Gamma_p = -(I/I_{\text{th}} - 1)\Gamma_g + 2\overline{Q}p$, describing the power fluctuations in the oscillator, and how the power fluctuations couple to the phase fluctuations through the nonlinear frequency shift N . It is of course this latter coupling that gives rise to the enhanced linewidth through the enhanced phase fluctuations. As we noted earlier, in the low-temperature limit, applicable here, the single-oscillator linewidth enhancement is described by the ratio of the nonlinear frequency shift N to the power restoration rate Γ_p : Power fluctuations couple to the nonlinear frequency shift, and the longer the decay time of power fluctuations is (*i.e.*, smaller Γ_p), the more power fluctuations can affect phase fluctuations. For the system under consideration here, Eqs. (8) and (9) show that the mode-coupling k leads to additional coupling between power and phase fluctuations. In general, the solutions to these equations, especially in the presence of thermal fluctuations, are complicated. We can, however, gain some insight by assuming that $\omega_{1,0} \approx \omega_{2,0}$ with $\omega_{2,0} > \omega_{1,0}$ and consider the system far from a mode transition so that k is small and $\theta = -\pi/2 + \delta$, with $\delta \ll 1$, and φ small and negative. For the nanocontact STOs, the nonlinear amplification N is large, and the nonlinear damping small. First, with N large and k small, we can neglect the terms in $\delta\psi$ on the right-hand side of Eq. (9). This means that power amplitude fluctuations couple to phase fluctuations through N just as for the single oscillator. It follows that if the power amplitude fluctuations are enhanced or prolonged by the mode coupling so that δp is enhanced or Γ_p reduced by the mode coupling, Second, for N large and the nonlinear damping small, at the fixed point $\theta \approx -\pi/2$ we have $\cos(\varphi - \Psi) \approx 0$ and $\sin(\varphi - \Psi) \approx -1$. If we neglect the terms in $\delta\psi$ on the right-hand side of Eq. (8), the net effect under these assumptions is to change the power restoration rate $\Gamma_p \rightarrow \Gamma_p - k \cos(\theta) \sin(|\varphi|)$ with a concomitant enhancement of the nonlinear amplification and the linewidth as the coupling term ν between power amplitude and phase fluctuations is given by $\nu = Np_0/\Gamma_p$ in single mode theory.³⁸ This explains qualitatively why the observed dependence of the linewidth on temperature in general does not agree with the theoretical expression³⁸ (Fig. 4). In the latter, the temperature dependence is driven by the stochastic thermal noise. In contrast, the experimentally determined nonlinear amplification contains a modified power restoration rate that includes the temperature (and current) dependence of k (and φ).

V. CONCLUSIONS

In conclusion, we have shown that the behavior of spin torque oscillator linewidths is to a large extent determined by nonlinearities arising from a number of mode transitions. The mode transitions are observed at increasing current at fixed temperature, or at increasing temperature at fixed current. Near the mode transitions, the linewidth increases substantially. Nevertheless, both the current and temperature dependence of the linewidth are well described by the analytical single-oscillator theory using the nonlinear amplification extracted from experimental data. In contrast, the temperature dependence of the linewidth near the mode transitions does not agree well with the single-oscillator analytical theory if the nonlinear amplification is calculated directly from the theory. The experimental data showed the presence of an additional mode where the nonlinear amplification is enhanced near the mode transitions. We have argued that a temperature-dependent mode coupling leads to reduction of the power restorations rate, and therefore an enhancement of the nonlinear amplification and of the linewidth, and that this at least qualitatively explains the anomalous temperature dependence of the linewidth near the mode transitions. These results are important for the understanding of linewidth in spin torque oscillators.

ACKNOWLEDGEMENTS

We thank Fred Mancoff at Everspin Technologies, USA for providing the samples used in this work. We also thank S. Bonetti and Niels de Vreede for assistance in experiments and useful discussions. Support from the Swedish Foundation for Strategic Research (SSF), the Swedish Research Council (VR), and the Göran Gustafsson Foundation are gratefully acknowledged. Knut and Alice Wallenberg foundation (KAW), is acknowledged for funding of the equipment used for measurements presented here. P. M. acknowledges Swedish Research Council (VR) for the "Junior Researchers Project Grant". J. Å. is a Royal Swedish Academy of Sciences Research Fellow supported by a grant from the Knut and Alice Wallenberg Foundation. Argonne National Laboratory is operated under Contract No. DE-AC02-06CH11357 by UChicago Argonne, LLC.

* pranaba.muduli@physics.gu.se

¹ J. C. Slonczewski, J. Magn. Magn. Mater., **159**, L1 (1996).

² L. Berger, Phys. Rev. B, **54**, 9353 (1996).

³ M. Tsoi, A. G. M. Jansen, J. Bass, W.-C. Chiang, M. Seck, V. Tsoi, and P. Wyder, Phys. Rev. Lett., **80**, 4281 (1998).

⁴ M. Tsoi, A. G. M. Jansen, J. Bass, W.-C. Chiang, V. Tsoi, and P. Wyder, Nature (London), **406**, 46 (2000).

⁵ S. I. Kiselev, J. C. Sankey, I. N. Krivorotov, N. C. Emley, R. J. Schoelkopf, R. A. Buhrman, and D. C. Ralph, Nature, **425**, 380 (2009).

- ⁶ D. C. Ralph and M. D. Stiles, *J. Magn. Magn. Mater.*, **320**, 1190 (2008).
- ⁷ J. Z. Sun and D. C. Ralph, *J. Magn. Magn. Mater.*, **320**, 1227 (2008).
- ⁸ T. J. Silva and W. H. Rippard, *J. Magn. Magn. Mater.*, **320**, 1260 (2008).
- ⁹ W. H. Rippard, M. R. Pufall, S. Kaka, T. J. Silva, and S. E. Russek, *Phys. Rev. B*, **70**, 100406 (2004).
- ¹⁰ S. Bonetti, P. Muduli, F. Mancoff, and J. Åkerman, *Appl. Phys. Lett.*, **94**, 102507 (2009).
- ¹¹ P. K. Muduli, O. G. Heinonen, and J. Åkerman, *J. Appl. Phys.*, **110**, 076102 (2011).
- ¹² S. Bonetti, V. Tiberkevich, G. Consolo, G. Finocchio, P. Muduli, F. Mancoff, A. Slavin, and J. Åkerman, *Phys. Rev. Lett.*, **105**, 217204 (2010).
- ¹³ V. E. Demidov, S. Urazhdin, and S. O. Demokritov, *Nat. Mater.*, **9**, 984 (2010).
- ¹⁴ M. Madami, S. Bonetti, G. Consolo, S. Tacchi, G. Carlotti, G. Gubbiotti, F. B. Mancoff, M. A. Yar, and J. Åkerman, *Nat. Nanotechnol.*, **6**, 635 (2011).
- ¹⁵ M. R. Pufall, W. H. Rippard, S. Kaka, T. J. Silva, and S. E. Russek, *Appl. Phys. Lett.*, **86**, 082506 (2005).
- ¹⁶ M. Manfrini, T. Devolder, J.-V. Kim, P. Crozat, N. Zerounian, C. Chappert, W. van Roy, L. Lagae, G. Hrkac, and T. Schrefl, *Appl. Phys. Lett.*, **95**, 192507 (2009).
- ¹⁷ P. K. Muduli, Y. Pogoryelov, S. Bonetti, G. Consolo, F. Mancoff, and J. Åkerman, *Phys. Rev. B*, **81**, 140408 (2010).
- ¹⁸ P. K. Muduli, Y. Pogoryelov, Y. Zhou, F. Mancoff, and J. Åkerman, *Integr. Ferroelectr.*, **125**, 147 (2011).
- ¹⁹ Y. Pogoryelov, P. K. Muduli, S. Bonetti, F. Mancoff, and J. Åkerman, *Appl. Phys. Lett.*, **98**, 192506 (2011).
- ²⁰ Y. Pogoryelov, P. K. Muduli, S. Bonetti, E. Iacocca, F. Mancoff, and J. Åkerman, *Appl. Phys. Lett.*, **98**, 192501 (2011).
- ²¹ M. Manfrini, T. Devolder, J.-V. Kim, P. Crozat, C. Chappert, W. van Roy, and L. Lagae, *J. Appl. Phys.*, **109**, 083940 (2011).
- ²² P. K. Muduli, Y. Pogoryelov, F. Mancoff, and J. Åkerman, *IEEE Trans. Magn.*, **47**, 1575 (2011).
- ²³ P. K. Muduli, Y. Pogoryelov, G. Consolo, F. Mancoff, and J. Åkerman, *AIP Conf. Proc.*, **1347**, 318 (2011).
- ²⁴ P. Villard, U. Ebels, D. Houssameddine, J. Katine, D. Mauri, B. Delaet, P. Vincent, M.-C. Cyrille, B. Viala, J.-P. Michel, J. Prouvee, and F. Badets, *IEEE J. Solid-State Circuits*, **45**, 214 (2010).
- ²⁵ B. Engel, J. Åkerman, B. Butcher, R. Dave, M. DeHerrera, M. Durlam, G. Grynkewich, J. Janesky, S. Pietambaram, N. Rizzo, J. Slaughter, K. Smith, J. Sun, and S. Tehrani, *IEEE Trans. Magn.*, **41**, 132 (2005).
- ²⁶ J. Åkerman, *Science*, **308**, 508 (2005).
- ²⁷ J. C. Sankey, I. N. Krivorotov, S. I. Kiselev, P. M. Braganca, N. C. Emley, R. A. Buhrman, and D. C. Ralph, *Phys. Rev. B*, **72**, 224427 (2005).
- ²⁸ Q. Mistral, J.-V. Kim, T. Devolder, P. Crozat, C. Chappert, J. A. Katine, M. J. Carey, and K. Ito, *Appl. Phys. Lett.*, **88**, 192507 (2006).
- ²⁹ B. Georges, J. Grollier, V. Cros, A. Fert, A. Fukushima, H. Kubota, K. Yakushijin, S. Yuasa, and K. Ando, *Phys. Rev. B*, **80**, 060404 (2009).
- ³⁰ C. Boone, J. A. Katine, J. R. Childress, J. Zhu, X. Cheng, and I. N. Krivorotov, *Phys. Rev. B*, **79**, 140404 (2009).
- ³¹ P. Bortolotti, A. Dussaux, J. Grollier, V. Cros, A. Fukushima, H. Kubota, K. Yakushiji, S. Yuasa, K. Ando, and A. Fert, *Appl. Phys. Lett.*, **100**, 042408 (2012).
- ³² J. F. Sierra, M. Quinsat, F. Garcia-Sanchez, U. Ebels, I. Joumard, A. S. Jenkins, B. Dieny, M.-C. Cyrille, A. Zeltser, and J. A. Katine, *Appl. Phys. Lett.*, **101**, 062407 (2012).
- ³³ M. L. Schneider, W. H. Rippard, M. R. Pufall, T. Cecil, T. J. Silva, and S. E. Russek, *Phys. Rev. B*, **80**, 144412 (2009).
- ³⁴ J.-V. Kim, *Phys. Rev. B*, **73**, 174412 (2006).
- ³⁵ J.-V. Kim, V. Tiberkevich, and A. N. Slavin, *Phys. Rev. Lett.*, **100**, 017207 (2008).
- ³⁶ J. V. Kim, Q. Mistral, C. Chappert, V. S. Tiberkevich, and A. N. Slavin, *Phys. Rev. Lett.*, **100**, 167201 (2008).
- ³⁷ V. S. Tiberkevich, A. N. Slavin, and J.-V. Kim, *Phys. Rev. B*, **78**, 092401 (2008).
- ³⁸ A. Slavin and V. Tiberkevich, *IEEE Trans. Magn.*, **45**, 1875 (2009).
- ³⁹ T. Silva and M. Keller, *IEEE Trans. Magn.*, **46**, 3555 (2010).
- ⁴⁰ M. W. Keller, M. R. Pufall, W. H. Rippard, and T. J. Silva, *Phys. Rev. B*, **82**, 054416 (2010).
- ⁴¹ S. Bonetti, V. Puliafito, G. Consolo, V. S. Tiberkevich, A. N. Slavin, and J. Åkerman, *Phys. Rev. B*, **85**, 174427 (2012).
- ⁴² P. K. Muduli, O. G. Heinonen, and J. Åkerman, *Phys. Rev. Lett.*, **108**, 207203 (2012).
- ⁴³ F. B. Mancoff, N. D. Rizzo, B. N. Engel, and S. Tehrani, *Appl. Phys. Lett.*, **88**, 112507 (2006).
- ⁴⁴ P. K. Muduli, O. G. Heinonen, and J. Åkerman, *Phys. Rev. B*, **83**, 184410 (2011).
- ⁴⁵ J. C. Slonczewski, *J. Magn. Magn. Mater.*, **195**, 261 (1999).
- ⁴⁶ A. Slavin and V. Tiberkevich, *Phys. Rev. Lett.*, **95**, 237201 (2005).
- ⁴⁷ W. H. Rippard, M. R. Pufall, and S. E. Russek, *Phys. Rev. B*, **74**, 224409 (2006).
- ⁴⁸ I. N. Krivorotov, D. V. Berkov, N. L. Gorn, N. C. Emley, J. C. Sankey, D. C. Ralph, and R. A. Buhrman, *Phys. Rev. B*, **76**, 024418 (2007).
- ⁴⁹ D. V. Berkov and N. L. Gorn, *Phys. Rev. B*, **76**, 144414 (2007).
- ⁵⁰ V. Tiberkevich, A. Slavin, and J.-V. Kim, *Appl. Phys. Lett.*, **91**, 192506 (2007).
- ⁵¹ A. N. Slavini and P. Kabos, *IEEE Trans. Magn.*, **41**, 1264 (2005).
- ⁵² A. Slavin and V. Tiberkevich, *IEEE Trans. Magn.*, **44**, 1916 (2008).
- ⁵³ G. van der Sande, L. Gelens, P. Tassin, and J. Scirè, A. aand Danckaert, *J. Phys. B: At. Mol. Opt. Phys.*, **41**, 095402 (2008).